Front. Energy 2025, 19(6): 969–984
https://doi.org/10.1007/s11708-025-1032-2

RESEARCH ARTICLE

Comprehensive analysis of alkaline earth metal ion removal from biodiesel using amino polycarboxylate chelating agents: Performance and mechanistic insights

Rongyan Li[1,3], **Xinru Han**[1,2,3], **Fashe Li** (✉)[1,2,3], **Shuang Wang** (✉)[1,3], **Meng Sui**[1,2,3], **Jing Yang**[4]

1 Yunnan Key Laboratory of Clean Energy and Energy Storage Technology, Kunming University of Science and Technology, Kunming 650093, China
2 State Key Laboratory of Complex Nonferrous Metal Resources Clean Utilization, Kunming University of Science and Technology, Kunming 650093, China
3 Faculty of Metallurgical and Energy Engineering, Kunming University of Science and Technology, Kunming 650093, China
4 Department of Applied Biology and Chemical Technology, The Hong Kong Polytechnic University, 999077 Hong Kong, China

Abstract The presence of alkaline earth metal ions in biodiesel can exacerbate engine wear, impair fuel oxidation stability, and substantially reduce combustion efficiency. Improving the quality of biodiesel is therefore crucial for promoting its adoption as a viable alternative to conventional fossil fuels. This study investigates the removal of alkaline earth metal calcium (Ca^{2+}) and magnesium (Mg^{2+}) from Jatropha biodiesel using four amino polycarboxylate chelating agents: ethylenediaminetetraacetic acid (EDTA), diethylenetriaminepentaacetic acid (DTPA), 1,2-cyclohexanediaminetetraacetic acid (CDTA), and N-(2-hydroxyethyl)-ethylenediaminetriacetic acid (HEDTA). The results showed that CDTA demonstrated the highest removal efficiency and selectivity for Ca^{2+} and Mg^{2+} among the four chelating agents, resulting in removal rates of 98.6% and 94.3%, respectively. Furthermore, the oxidative stability of biodiesel, measured as induction period, increased from 3.38 to 8.31 h after treatment with EDTA solution and reached a maximum of 8.68 h after treatment with CDTA. Density functional theory (DFT) calculations were performed to analyze Mulliken charges, electrostatic potential, frontier molecular orbitals, and interaction energies. The results indicate that the four chelating agents form cyclic structure complexes by simultaneously coordinating with a metal ion through multiple coordination atoms (N atom in amino group and O atom in carboxyl group). CDTA has the strongest interaction energies with Ca^{2+} and Mg^{2+}, calculated at –826 and –915 kcal/mol, respectively, corroborating its superior chelation performance.

Keywords chelation mechanism, Jatropha biodiesel, impurity ions, oxidation stability

1 Introduction

The increasing global energy demand has accelerated the depletion of fossil fuel reserves, highlighting the urgent need to search for clean and renewable energy alternatives [1,2]. Biodiesel, as a recognized green and sustainable fuel, has emerged as a research hotspot due to its advantages such as widespread availability and low environmental pollution [3,4]. However, during biodiesel production, storage, and transportation, alkali and alkaline earth metal ions are often introduced due to the nature of feedstock sources and complex storage conditions for synthesis [5,6]. In many biodiesel samples, the concentrations of these metal ions significantly exceed the permissible threshold of 5 mg/kg, as stipulated in different standards such as GB 25199-2017, ASTM D 675115c, and EN14214:2012 + A2:2019 [7]. Elevated levels of these ions lead to the formation of insoluble soaps and abrasive solid byproducts during combustion, which accelerate engine wear and degrade biodiesel properties [8–10]. Consequently, it is crucial to reduce ion content to accelerate the utilization of biodiesel as a viable alternative to traditional diesel fuels [11].

A series of studies have been conducted exploring various strategies for the removal of alkaline earth metal ions, including foam flotation, selective adsorption, and

Received Mar. 3, 2025; accepted Jun. 5, 2025; online Jul. 28, 2025
Correspondences: Fashe Li, lifashe@kust.edu.cn;
Shuang Wang, wxy_ws@kust.edu.cn

solvent extraction. For instance, Matsuoka et al. [12] used foam separation to remove dissolved alkaline earth metal ions from aqueous solutions. Yu et al. [13] and Cui et al. [14] utilized water soaking or washing to remove water-soluble inorganic species such as K, Na, Ca, Cl, and Mg from biomass feedstocks. Gao et al. [15] and Luo et al. [16] used resin adsorption to remove alkali and alkaline earth metal ions, while Wang and Lin [17] selectively removed Ca^{2+} from water using capacitive deionization (CDI) technology.

Despite their merits, these methods have notable limitations. Froth flotation demonstrates poor separation efficiency for dissolved ionic species and requires complex pretreatment requirements. Adsorption methods are constrained by low capacity and inadequate selectivity, while ion-exchange resins exhibit vulnerability to organic fouling, with their exchange capacity being strictly pH-dependent. In contrast, solvent extraction is a process that only produces trace amounts of secondary pollutants, and has been regarded as a green method for ionic removal.

Chelating agents, first introduced by Morgan and Drew in the 1920s [18], are compounds containing two or more ligands capable of donating electrons to form coordination bonds with a central metal atom. As a clean and efficient extraction technology, it has been widely applied in wastewater treatment [19], polluted soil remediation [20], treatment of heavy metal poisoning [21], and the upstream oil and gas industry [22,23]. For instance, Wang et al. [24] demonstrated that chelating agents form stable complexes with alkaline earth metal cations, effectively removing scale deposits from subsurface equipment. Li et al. [25] reported that chelating agents increase the solubility of inorganic scales and prevent precipitation caused by ionic recombination through effective metal ion binding. Edmunds et al. [26] evaluated the ion extraction efficiencies of ethylenediaminetetraacetic acid (EDTA), citric acid, acetic acid, sulfuric acid, and water, while Sorour et al. [27] confirmed the efficacy of diverse chelating agents in removing Ca^{2+} and Mg^{2+} ions from seawater, highlighting their adaptability in complex ionic environments.

The studies collectively demonstrate that both EDTA and ethylene glycol bis(2-aminoethyl ether)-*N*,*N*,*N*′,*N*′-tetraacetic acid (EGTA) exhibited enhanced chelation performance toward these divalent cations, suggesting their structural adaptability in complex ionic matrices. These studies indicate that chelating agents have the superior performance in improving biomass quality via efficiently and selectively removing inorganic substances and extracting heavy metals from water. A key advantage of chelating agents lies in their structural tunability, which allows for optimum selectivity and extraction efficiency toward specific metal cations, even at very low ion concentrations [28]. However, the integrated application of chelation and solvent extraction for ionic contaminant removal in biodiesel refining remains scarcely explored.

In comparison with other types of chelating agents, amino polycarboxylate chelating agents (APCAs) exhibit significant advantages due to their unique molecular structure. These compounds are characterized by multiple carboxy (COO^-) groups connected to one or more N atoms via carbon backbones, structurally resembling derivatives of the amino acid glycine [29]. APCAs can form a multidentate coordination structure with metal ions by providing 4 to 6 coordination sites, resulting in stable complexes with five-membered or six-membered ring structures [30]. This multidentate synergistic effect enables the formation of stable complexes with metal ions, have the potential to reduce alkaline earth metal concentrations in biodiesel, thereby improving its quality. These properties make APCAs ideal candidates for chelation extraction.

In this study, four APCAs, ethylenediaminetetraacetic acid (EDTA), N-(2-hydroxyethyl)-ethylenediaminetriacetic acid (HEDTA), 1,2-cyclohexanediaminetetraacetic acid (CDTA), and diethylenetriaminepentaacetic acid DTPA were selected to investigate their effectiveness in removing Ca^{2+} and Mg^{2+} ions from Jatropha-derived biodiesel based on their chemical properties and selectivity for metal ion impurities. A comprehensive analysis was conducted to unravel the chelation mechanisms of different chelating agents on alkaline earth metal ions and their impact on the properties of biodiesel. Potential complexation reactions between Ca^{2+}, Mg^{2+}, and the APCAs were explored to elucidate the underlying chelation mechanisms, providing insights into the design of more efficient biodiesel purification strategies.

2 Materials and methods

The Jatropha biodiesel used in this study was synthesized in-house using a conventional transesterification process. Jatropha crude oil, methanol (analytical reagent grade (AR), ⩾ 99.5%), and potassium hydroxide (AR, ⩾ 85.0%) were purchased from Yunnan Yingding Bioenergy Co., Ltd., China, Tianjin Dingshengxin Chemical Industry Co., Ltd., China, and Tianjin Fengchuan Chemical Reagent Technology Co., Ltd., China, respectively.

In a typical procedure, Jatropha crude oil and methanol were mixed in a 1:2.2 molar ratio in a 1000 mL round-bottom flask, followed by the addition of an appropriate amount of potassium hydroxide catalyst. The mixture was placed in a water bath at a constant temperature of 85 °C for 120 min to react. The resulting crude biodiesel was transferred to a 500 mL separatory funnel and washed multiple times with deionized water to remove impurities. After allowing the mixture to settle for 30 min

to facilitate phase separation, the biodiesel layer was dried using a rotary evaporator under reduced pressure to remove excess water. Finally, the final biodiesel was filtered through qualitative filter paper to obtain the purified biodiesel.

2.1 Extraction

The workflow for metal ion extraction is illustrated in Fig. 1. Aqueous solutions of four chelating agents, HEDTA, EDTA, CDTA, and DTPA were prepared at concentrations of 0.3‰, 0.9‰, 1.5‰, and 2.1‰, respectively. For each extraction experiment, 26 g of Jatropha biodiesel was accurately weighed using an analytical balance (precision: 0.0001 g) and transferred into a 100 mL beaker. Subsequently, 30 mL of the respective chelating agent solution was added, and the mixture was subjected to liquid–liquid extraction (LLE) via vortex agitation for 1 h. This mixing duration was previously optimized to ensure maximal extraction efficiency.

After mixing, the oil-water mixture was transferred to a separatory funnel and left undisturbed for 5 min to facilitate phase separation. The lower aqueous phase was collected into a 200 mL volumetric flask, while the upper biodiesel layer was returned to the beaker for subsequent washing. This extraction and separation process was repeated five times, each using 30 mL of fresh chelating agent solution. All extractions were performed at a controlled ambient temperature was of 25 °C.

After the final wash, all aqueous extracts were combined, diluted to a final volume of 200 mL with ultrapure water, and mixed thoroughly. The resulting solution was then analyzed for Ca^{2+} and Mg^{2+} ion concentrations using an ion chromatograph.

The chelating agents used were sourced as follows: EDTA (AR, ⩾ 99%) from Fuchen Chemical Reagent Co., Ltd. (Tianjin, China); HEDTA (AR, 98%) from Aladdin (Shanghai, China); and CDTA (AR, 98%) and DTPA (AR, ⩾ 99%) from Macklin Biochemical Co., Ltd. (Shanghai, China).

2.2 Characterization

2.2.1 Ion chromatography for elemental analysis

The concentration of alkaline earth metal ions in biodiesel was quantified using an ion chromatography system (883 Basic IC Plus, Metrohm AG, Switzerland). This system is equipped with a dual-pump mechanism, an online filter, a pulse damper, and the 863 Compact Autosampler. Operation and data acquisition were managed via the Mag IC Net Basic software integrated with the IC Net 3.1 workstation. Figure 2 illustrates the working principle of cation analysis using ion chromatography, which involves five key components: the infusion system, sample injection system, separation system, detection system, and data processing interface.

During analysis, the high-pressure pump delivers the mobile phase at a constant pressure to the analytical system, propelling the sample, introduced via an injection value, into the chromatographic column. Inside the column, the ions are separated based on their affinity with the stationary phase and eluted sequentially with the mobile phase toward the detector.

The key specifications of the ion chromatograph are as

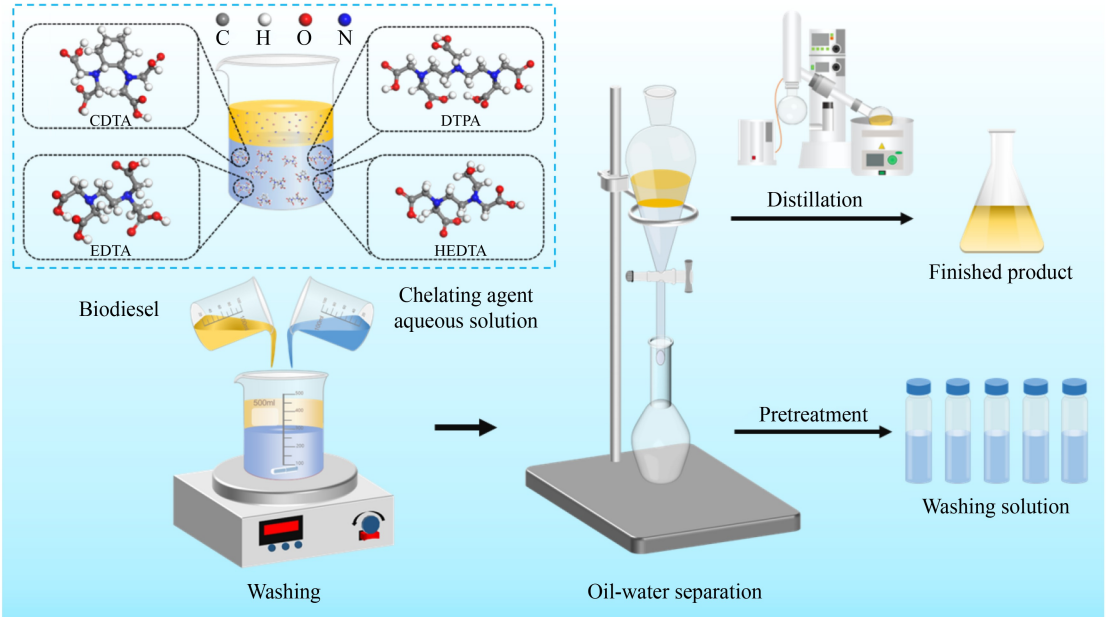

Fig. 1 Schematic diagram and workflow of extraction.

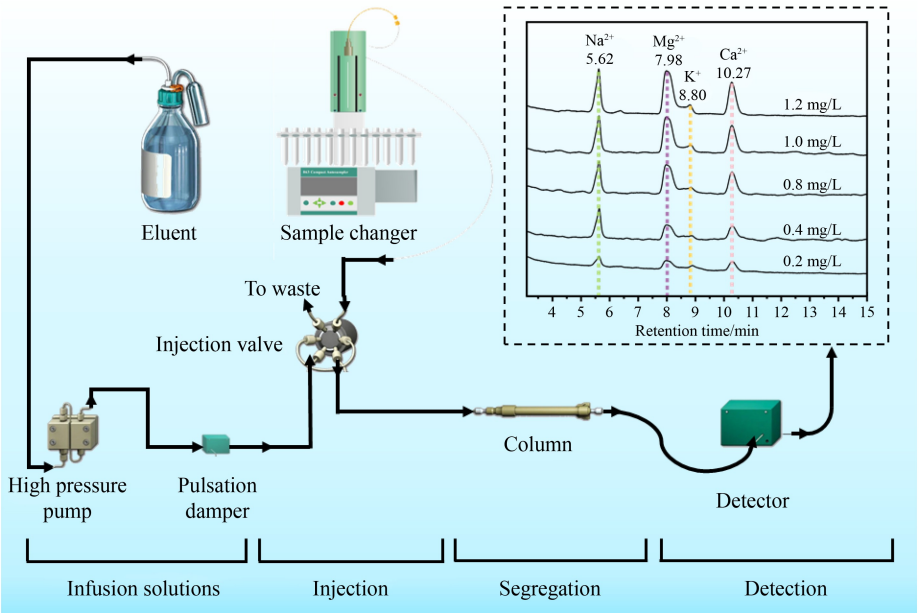

Fig. 2 Schematic of the ion chromatography cation analysis working principle.

follows: noise < 0.1 nS (within 1 μS/cm); temperature stability < 0.001 °C; resolution 0.0047 nS/cm; baseline noise < 0.2 nS/cm; measurement range 0–15000 Sc; and linear deviation < 0.1% [31].

Deionized water (MilliQ, Millipore) was used for the preparation of eluents and samples solutions, while ultrapure nitric acid (0.05%, BASF) served as the washing solution for system maintenance and contamination prevention.

The filtered sample solution was prepared as outlined in Section 2.1, using a Cleanert® SPE C18 reverse-phase column in conjunction with a Clarinert™ 0.22 μm nylon filter to remove oils and macromolecules. The resulting filtered solution was then analyzed using ion chromatography [16]. Each sample was measured three times, and the average value was calculated to ensure analytical accuracy and reproducibility.

2.2.2 Oxidative stability test

The oxidative stability of biodiesel was evaluated using a Rancimat instrument (Rancimat 873 biodiesel oxidative stability tester, Metrohm AG, Switzerland) in accordance with the EN 14112-2003 standard [32]. For each test, 3 g of biodiesel was accurately weighed and placed into a sample vessel, which was then maintained at a constant temperature of 110 °C. Air was continuously supplied at a constant flow rate of 10 L/h to accelerate oxidation. The resulting volatile oxidation products were transported by the airflow into a measuring vessel containing ultrapure water, where the formation of secondary oxidation products caused a measurable increase in water conductivity.

The change in conductivity was monitored in real time, and the induction period, defined as the point of inflection in the second derivative of the conductivity curve, was used as a quantitative indicator of the oxidative stability of the biodiesel [33]. A typical conductivity profile and its second derivative curve are shown in Fig. 3.

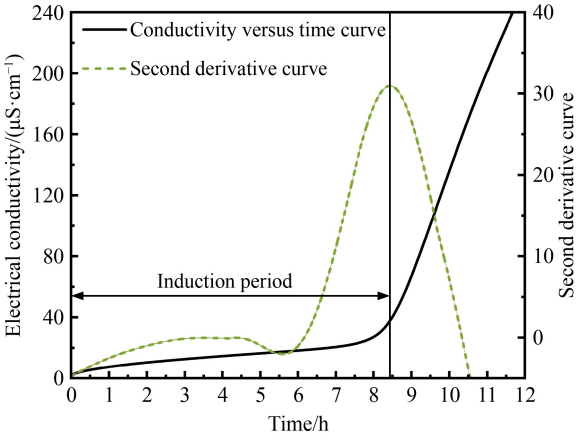

Fig. 3 Definition of oxidation induction period.

2.3 Chelation chemistry

Chelating agents are anionic organic molecules that coordinate with metal ions through multiple coordination bonds. During chelation, these agents form stable cyclic structures by fully occupying the coordination sites of the metal ion, thereby preventing further interactions with other metal ions or molecules in solution. The stability of

a metal-ligand complex is influenced by the intrinsic properties of both the metal ion and the chelating agent. APCAs are particularly effective in forming strong and stable complexes with alkaline earth metal ions, such as Ca^{2+} and Mg^{2+} [34].

Table 1 [36,37] presents the chemical structures of HEDTA, EDTA, CDTA, and DTPA, along with their stability constants (log K_{MY}) for complexes with Ca^{2+} and Mg^{2+}. A higher stability constant indicates a stronger and more stable chelate [35].

The formation of metal-ligand complexes by the following equilibrium reactions,

$$M^{n+} + Y^{x-} \rightleftarrows MY^{n-x} \quad (1)$$

$$K_{MY} = \frac{[MY^{n-x}]}{[M^{n+}][Y^{x-}]} \quad (2)$$

where M^{n+}, Y^{x-}, $MY^{(n-x)}$, and log K_{MY} refer to the central metal ion, chelating ligand, formed complex, and the logarithmic form of K_{MY}, respectively.

These chelating agents form stable complexes with Ca^{2+} and Mg^{2+}, with log K_{MY} values typically exceeding 8. Under standard conditions, CDTA, DTPA, HEDTA, and EDTA form one-to-one stoichiometric complexes with most metal ions [38]. The denticity of a chelating ligand, i.e., the number of donor atoms available for coordination with the central metal ion, determines the stability and complexity of the resulting complex. A higher denticity increases the number of coordination sites available, leading to more stable and intricate complexes. HEDTA, EDTA, CDTA, and DTPA possess coordination numbers of 5, 6, 6, and 8, respectively. These donor atoms include both carboxylate oxygen atoms and nitrogen atoms in each ligand.

However, denticity does not always correspond directly to the number of actual coordination bonds formed, as this depends on the coordination preferences of the specific metal ion involved. Although EDTA and CDTA share identical denticity, CDTA features a distinct cyclic structure compared to the other three chelators, possibly offering enhanced steric stability that may optimize metal-ligand coordination efficiency.

Figure 4 illustrates the idealized structures of the complexes formed by these chelating agents and divalent alkaline earth metal ions.

2.4 Calculation method

Periodic density functional theory (DFT) calculations are widely used to investigate the interactions between compounds and metal complexes, including those involving chelating agents and metal ions in the petroleum and natural gas industries [39–41]. In this study, DFT calculations were conducted using the Dmol^3

Table 1 Chemical structures and stability constants for HEDTA, EDTA, CDTA, and DTPA with Ca^{2+} and Mg^{2+} at 25 °C

Compound	Molecular formula	Denticity	Structural formula	log K_{MY}	
				Ca^{2+}	Mg^{2+}
HEDTA	$C_{10}H_{18}O_7N_2$	5	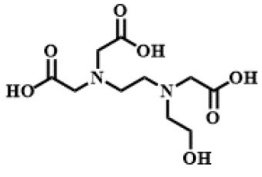	8.4	7.0
EDTA	$C_{10}H_{16}O_8N_2$	6	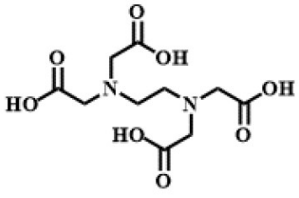	10.7	8.7
CDTA	$C_{14}H_{22}O_8N_2$	6	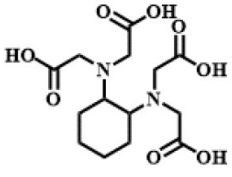	12.3	11.3
DTPA	$C_{14}H_{23}O_{10}N_3$	8	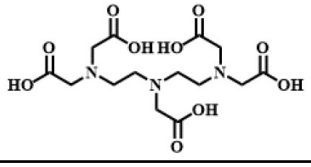	10.9	9.3

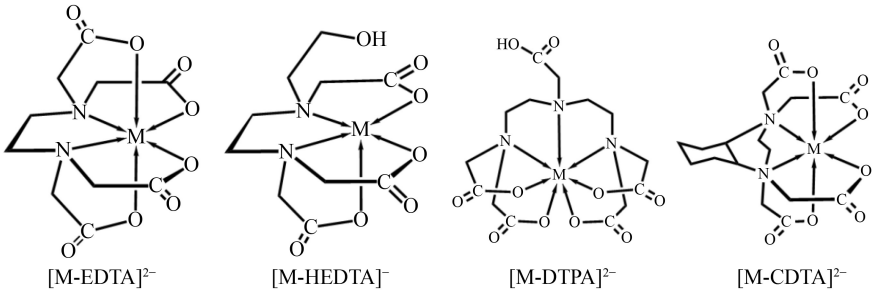

Fig. 4 Idealized structures of the complexes formed by four chelating agents with divalent alkaline earth metal ions.

module in the Materials Studio software suite [42,43]. The geometrical properties of all chelating agents were optimized to investigate their electronic interactions and coordination behaviors, using the generalized gradient approximation (GGA) [44] with the Becke exchange plus Lee-Yang-Parr correlation (BLYP) [45].

The structural and electronic properties of Ca^{2+} and Mg^{2+} complexes with EDTA, HEDTA, CDTA, and DTPA were systematically analyzed to elucidate the molecular binding mechanisms of chelating agents with alkaline earth metal ions [40]. Convergence thresholds for energy, maximum force, and maximum atomic displacement were set as follows: energy = 1×10^{-5} Ha, maximum force = 0.002 Ha/Å, and maximum atomic displacement = 0.005 Å, respectively.

The interaction energy (E_{int}) between the ligand and metal ion was calculated using Eq. (3)

$$E_{int} = E_{complex} - (E_{Ligand} + E_{M^{2+}}), \quad (3)$$

where E_{int} (Hartree) is the interaction energy, $E_{complex}$ (Hartree) is the electronic energy of the optimized complex, E_{Ligand} (Hartree) is the electronic energy of the free ligand, and $E_{M^{2+}}$ (Hartree) is the electronic energy of the divalent metal ion (Ca^{2+} or Mg^{2+}). A more negative E_{int} indicates a stronger interaction between the chelating agent and the metal ion. Table 2 provides the energies associated with the coordination interactions of the ligands with the metal ions.

Table 2 Interaction energies of APCAs with metal cations

		HEDTA	EDTA	CDTA	DTPA
Int. Energy	Ca^{2+}	−676.3309	−814.6134	−826.9716	−775.8283
	Mg^{2+}	−769.0957	−901.7438	−915.4681	−860.9387

3 Results and discussion

3.1 Effect of chelating agents on alkaline earth metal ion removal

Prior to formal testing, it is necessary to establish a calibration curve using standard solutions with five different gradient concentrations. Table 3 lists the retention time, linear equation, and correlation coefficient for Na^+, Mg^{2+}, K^+, and Ca^{2+}. The linear equation converts the signals obtained by the instrument into actual ion concentrations, enabling accurate quantitative analysis.

Table 3 Retention times, linear equations, and correlation coefficient for cations in ion chromatography

Ion	Retention time/min	Linear equation $A = a + bQ$		r
		a	b	
Na^+	5.62	1.74E–02	1.29E–02	0.999
Mg^{2+}	7.98	2.23E–02	2.23E–02	0.999
K^+	8.80	1.39E–02	1.60E–03	0.998
Ca^{2+}	10.27	6.26E–02	1.20E–02	0.998

Notes: A is the peak area, μS·min/cm; Q is the analyte concentration, mg/L; a and b are constants; and r is the correlation coefficient.

The concentrations of alkaline earth metal ions in Jatropha biodiesel, as determined using ICP-OES, were 5.38 mg/kg for Ca^{2+} and 2.97 mg/kg for Mg^{2+}, both exceeding the 5 mg/kg threshold specified by the EN14214:2012 + A2:2019 European standard. General water washing extracted a total Mg^{2+} and Ca^{2+} concentration of 4.67 mg/kg. Figure 5 compares the concentrations of alkaline earth metal ions extracted from Jatropha biodiesel with varying amounts of chelating agents (CDTA, EDTA, DTPA, and HEDTA). The results indicate that the addition of chelating agents significantly influences the concentrations of Ca^{2+} and Mg^{2+}.

The Mg^{2+} content in the aqueous solutions initially increased with the concentration of chelating agents, peaking at a 1.5 ‰ concentration before decreasing. In contrast, the Ca^{2+} content extracted was significantly higher than that achieved with general water washing. The highest Ca^{2+} concentrations were observed with 0.3 ‰ HEDTA, 0.9 ‰ DTPA, 0.9 ‰ CDTA, and 2.1 ‰ EDTA solutions. EDTA and HEDTA exhibited more pronounced chelation effects on Ca^{2+} at higher concentrations (1.5 ‰ and 2.1 ‰), while DTPA demonstrated greater effectiveness at lower concentrations (0.3‰).

The extraction performance of chelating agents at different concentrations is depicted in Fig. 6. General water washing extracted only 59.14% of Ca^{2+} and

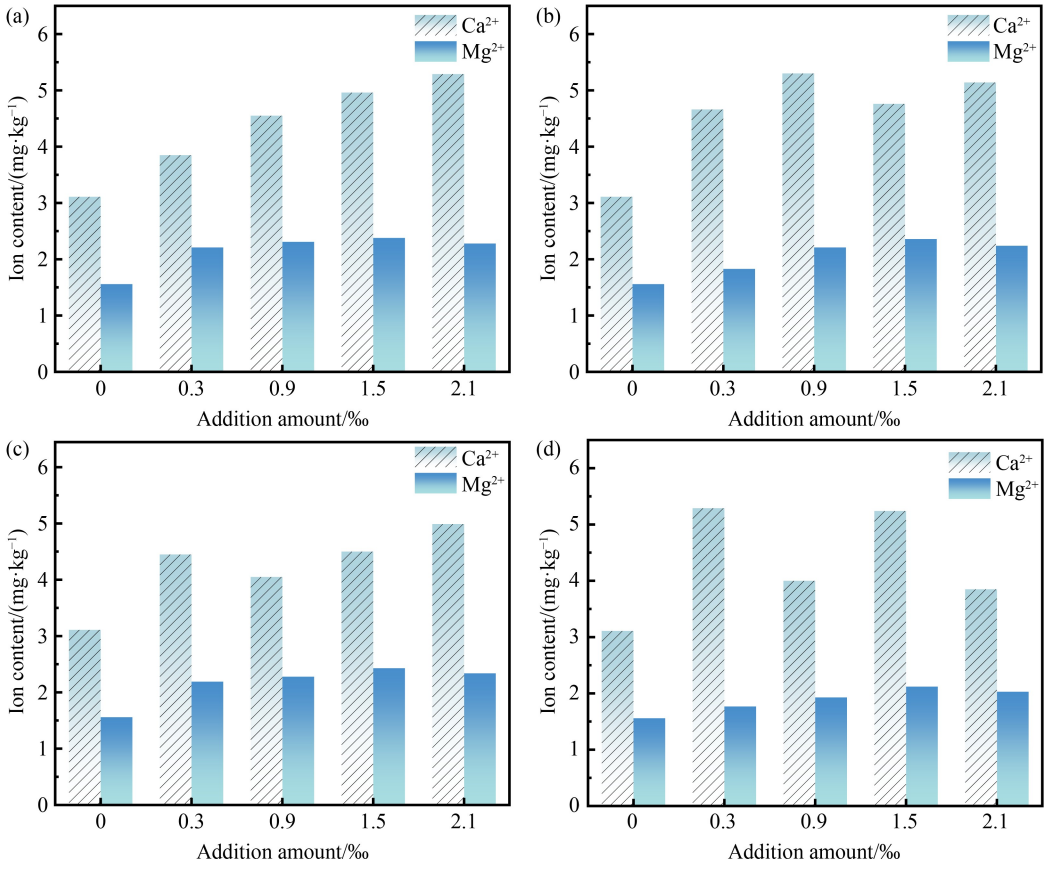

Fig. 5 Extraction of Ca^{2+} and Mg^{2+} from Jatropha biodiesel using various concentrations of chelating agents. (a) EDTA; (b) CDTA; (c) HEDTA; (d) DTPA.

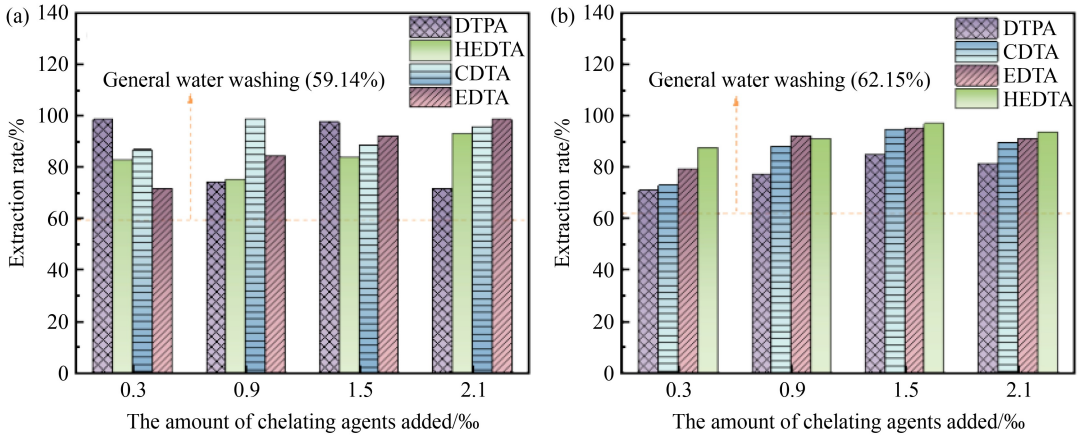

Fig. 6 Extraction rates with different concentrations of chelating agents. (a) Ca^{2+}; (b) Mg^{2+}

62.15% of Mg^{2+}. The addition of chelating agents significantly enhanced the extraction efficiency of alkaline earth metal ions. Among the chelating agents tested, CDTA exhibited the highest efficiency for Ca^{2+} removal, achieving extraction rates above 80% across all evaluated concentrations. A maximum Ca^{2+} extraction rate of 98.61% was achieved at 0.9 ‰ CDTA, while Mg^{2+} extraction peaked at 94.36% with 1.5‰ CDTA. In comparison, EDTA and DTPA showed relatively lower efficiencies for both Ca^{2+} and Mg^{2+} extraction. At higher concentrations (1.5‰ and 2.1‰), EDTA consistently achieved higher Ca^{2+} extraction rates than CDTA and HEDTA. However, for Mg^{2+}, the relative extraction efficiency followed the order HEDTA > EDTA > CDTA >

DTPA, with notable efficiency achieved at concentrations of 1.5‰ and 2.1‰.

In summary, chelating agents substantially improve the extraction efficiency of Ca^{2+} and Mg^{2+}, outperforming general water washing. Among the four amino polycarboxylate chelating agents examined, EDTA and CDTA demonstrate the most outstanding performance. This improvement is attributed to the ability of chelating agents to form stable coordination complexes with Ca^{2+} and Mg^{2+}, thereby increasing their solubility in water. In contrast, general water washing is limited to removing water-soluble ions and is ineffective against organic salts with low solubility. Although the use of amino polycarboxylate chelating agents proves highly effective, it is hindered by challenges such as complex synthesis processes, high costs, and limited biodegradability. From a sustainability perspective, further consideration should be given to the recycling and reuse of these chelating agents.

Table 1 presents the chelation constants (log K) for Ca^{2+} and Mg^{2+} with the four chelating agents, in the order of log K(CDTA) > log K(DTPA) > log K(EDTA) > log K(HEDTA). CDTA demonstrated the strongest affinity for both Ca^{2+} and Mg^{2+}. Based on these constants, CDTA and DTPA were theoretically expected to outperform EDTA and HEDTA in extracting these ions. However, experimental results (Fig. 5) showed that the average Ca^{2+} extraction efficiency followed the order of CDTA > EDTA > DTPA > HEDTA, while for Mg^{2+}, the order was HEDTA > EDTA > CDTA > DTPA. These findings differ from the ranking of the stability constants due to competing factors between the two coexisting ions and in the biodiesel-water mixture, particularly pH variations in the liquid phase. Shifts in the solution pH may affect the concentrations of aqueous metal species, the stability of metal chelates, the solubility of chelating agents, and the dynamics of metal sorption/desorption and ion exchange, leading to discrepancies between observed efficiencies and theoretical expectations.

3.2 Effect of ligand type and concentration on alkaline earth metal ions

Visual MINTEQ software was used to analyze the chemical species of Ca, Mg, and the four chelating ligands in aqueous solutions across varying pH levels. As shown in Figs. 7(a) and 7(b), calcium exists predominantly as Ca^{2+} at pH values below 11. Beyond pH 12.2, Ca^{2+} begins to precipitate as $Ca(OH)_2$, reducing the concentration of free calcium. Similarly, magnesium predominantly exists as Mg^{2+} at pH values below 10.48 but precipitates as $Mg(OH)_2$ at higher pH values. At pH 14.80, both ions are nearly absent from the solution due to complete precipitation.

The chelating agents exist in different forms depending on the pH, as shown in Figs. 7(c)–7(f). In the pH range of 3–7, ligands with two negative charges are predominantly present. APCAs undergo a stepwise deprotonation process to achieve their fully ionized state. The dissociation reactions of APCAs (H_mY) proceed are as follows

$$H_mY \rightleftarrows H_{m-1}Y^- + H^+ \quad (4)$$

$$H_{m-1}Y^- \rightleftarrows H_{m-2}Y^{2-} + H^+ \quad (5)$$

$$H_{m-2}Y^{2-} \rightleftarrows H_{m-3}Y^{3-} + H^+ \quad (6)$$

This stepwise dissociation continues until the chelating agent reaches its fully ionized state. In this context, H_mY represents the chelating agent molecule, where m denotes the number of replaceable hydrogen ions. For EDTA and CDTA, m equals 4, while for DTPA and HEDTA, m equals 5.

The distribution of ion species is governed by the equilibrium constants of each dissociation reaction and the pH of solution. The observed results can be explained as follows: within the pH range of 3–7, EDTA and CDTA predominantly exist in the H_2Y^{2-} form, HEDTA mainly exists in the H_2Y^- form, while DTPA exists in three distinct ligand forms. At higher pH values, CDTA and EDTA undergo sequential deprotonation, forming HY^{3-} and Y^{4-}, respectively. The ion distribution of CDTA closely resembles that of EDTA, consistent with findings reported in Fredd and Fogler [46]. In contrast, under low pH conditions, the ion distribution of DTPA is more complex. At pH 4, DTPA is primarily in the H_3Y^{2-} form, while at the pH range of 7–9, it predominantly exists as H_2Y^{3-}.

However, an increase in pH does not always enhance complex formation due to the competition between hydroxide ions and the ligand for binding to the metal ion. The pH at which maximum complexation occurs is influenced by both the acidity of the ligand and the affinity of the metal ion for hydroxide ions.

APCAs form complexes with metal ions most efficiently in basic solutions, as increased pH levels lead to full deprotonation of the chelating agents, thereby maximizing their chelating ability. In acidic conditions, chelating agents remain in their protonated forms, resulting in reduced chelation efficiency [46]. However, excessively high pH levels may hinder complex formation due to competition between hydroxide ions and the chelating agents for metal binding. Additionally, under strong alkaline conditions, biodiesel may undergo saponification reactions, which can compromise its quality.

To avoid such adverse effects, the experimental conditions in this study were maintained within a narrow pH range of 2–6 (as shown in Table 4). It was further observed that the pH of the chelating agent solutions tended to decrease as the concentration of agent increased.

To better understand chelation behavior under acidic conditions, the effect of chelating agent ligands on Ca^{2+}

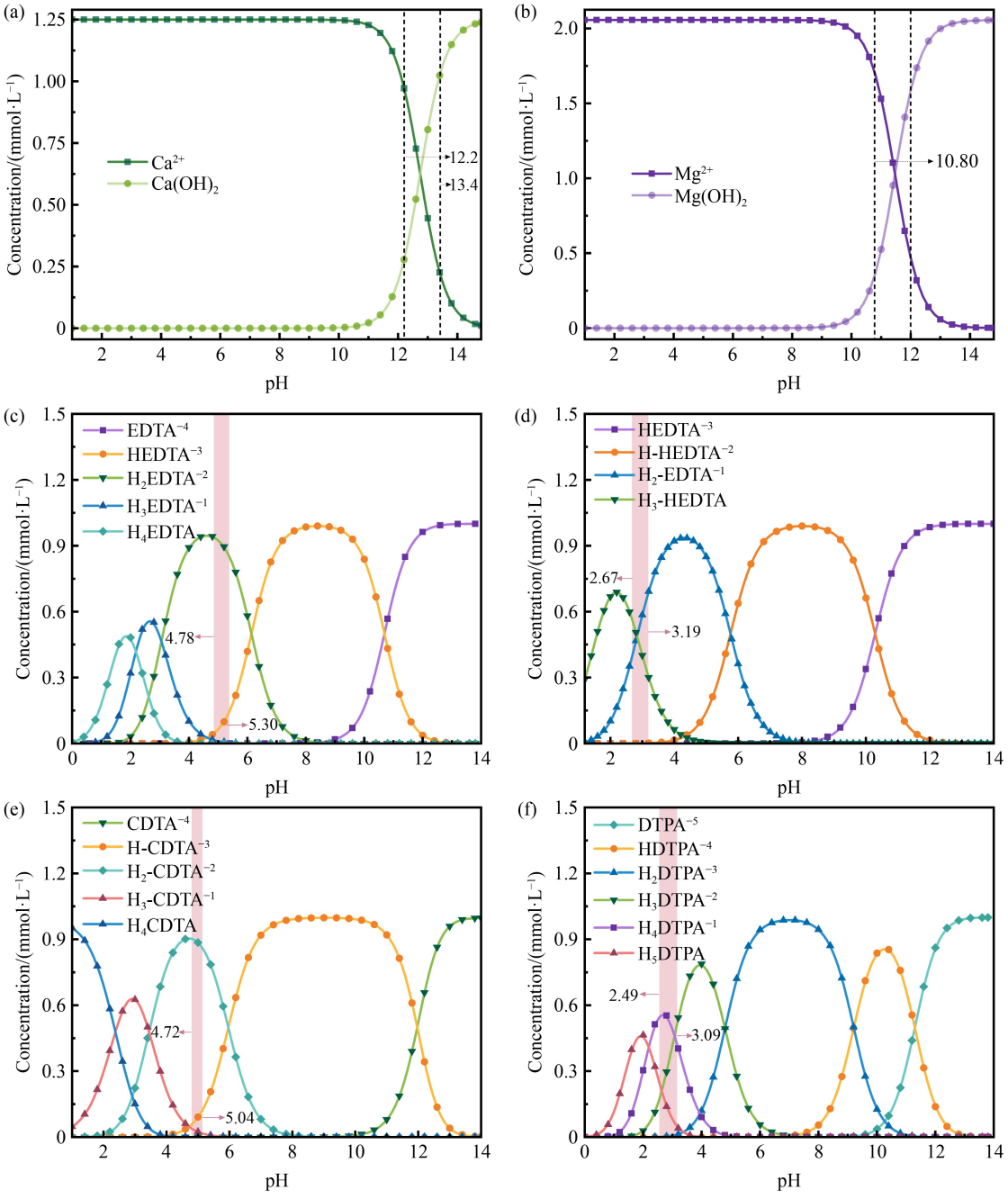

Fig. 7 Distribution of (a) Ca^{2+}, (b)Mg^{2+}, (c) EDTA, (d) HEDTA, (e) CDTA, and (f) DTPA at different pH values simulated by Visual MINTEQ software.

Table 4 pH of the washing solution at 25 °C

Concentration	EDTA	DTPA	CDTA	HEDTA
0.3‰	5.31	3.09	5.04	3.19
0.9‰	4.92	2.75	4.86	2.85
1.5‰	4.82	2.58	4.78	2.72
2.1‰	4.78	2.49	4.72	2.61

and Mg^{2+} was examined. As shown in Figs. 7(c)–7(f), EDTA predominantly exists as H_2Y^{2-} within a pH range of approximately 4.6–5.31, while CDTA primarily exists in the H_2Y^{2-} form in a pH range of approximately 4.7–6.0. The ion distribution of DTPA is more complex: at lower pH, it exists mainly as H_4Y^{-} at a pH of approximately 2.67, transitioning to H_3Y^{2-} between pH 3–4.8. Furthermore, HEDTA undergoes successive deprotonation to form H_2Y^{-} at low pH and remains in this form in the pH range of 2–3.5.

In summary, under mildly acidic conditions, Ca^{2+} and Mg^{2+} are primarily coordinated by $H_{m-2}Y^{2-}$ species of

EDTA, CDTA, and HEDTA. For DTPA, coordination involves H_2Y^{2-} and, to a lesser extent, H_3Y^{-}. To sum up, the concentration of the chelating agent affects the pH of the solution, which in turn alters the morphology of the ligands. Change in ligand morphology are likely to contribute to the observed variations in metal ion extraction performance.

3.3 Effect of chelating agents on the oxidative stability of biodiesel

Figure 8 illustrates the change in the oxidative induction period (OIP) of biodiesel after washing with chelating agent solutions at increasing concentrations. The initial OIP of untreated biodiesel is less than 6 h, failing to meet the GB 25199-2017 standard. Following treatment with CDTA, the oxidation stability of Jatropha biodiesel improved significantly, with the induction period extending from 3.38 h to a maximum of 8.68 h, thereby meeting the EN14214:2012 + A2:2019 (8 h). After treatment with the other three APCAs, the oxidation induction period of the Jatropha biodiesel was also significantly increased, meeting the GB 25199-2017 Standard of China (6 h).

This improvement demonstrates that washing biodiesel to remove alkaline earth metals enhances its oxidative stability. Biodiesel, as a multicomponent fuel comprised of saturated and unsaturated fatty acid esters [47], is susceptible to oxidation catalyzed by alkaline earth metal ions [48]. These ions are known to shorten the induction period of biodiesel [49]. Once chelating agent form complexes with these metal ions, the concentration of alkaline earth metal ions in Jatropha biodiesel from the leprosy tree is significantly reduced. This reduction effectively delays and inhibits the catalytic activity of alkaline earth metals on the oxidation products of fatty acid methyl esters, thereby slowing down catalytic oxidation and extending the oxidation induction period.

3.4 FTIR analysis

As shown in Fig. 9, the basic functional groups of biodiesel treated with chelating agents did not undergo significant changes compared to untreated Jatropha biodiesel. However, the intensity of these functional groups exhibited slight fluctuations. A broad and strong absorption peak at 3463 cm^{-1} corresponds to the O–H stretching vibration. The characteristic peak at 3008 cm^{-1}

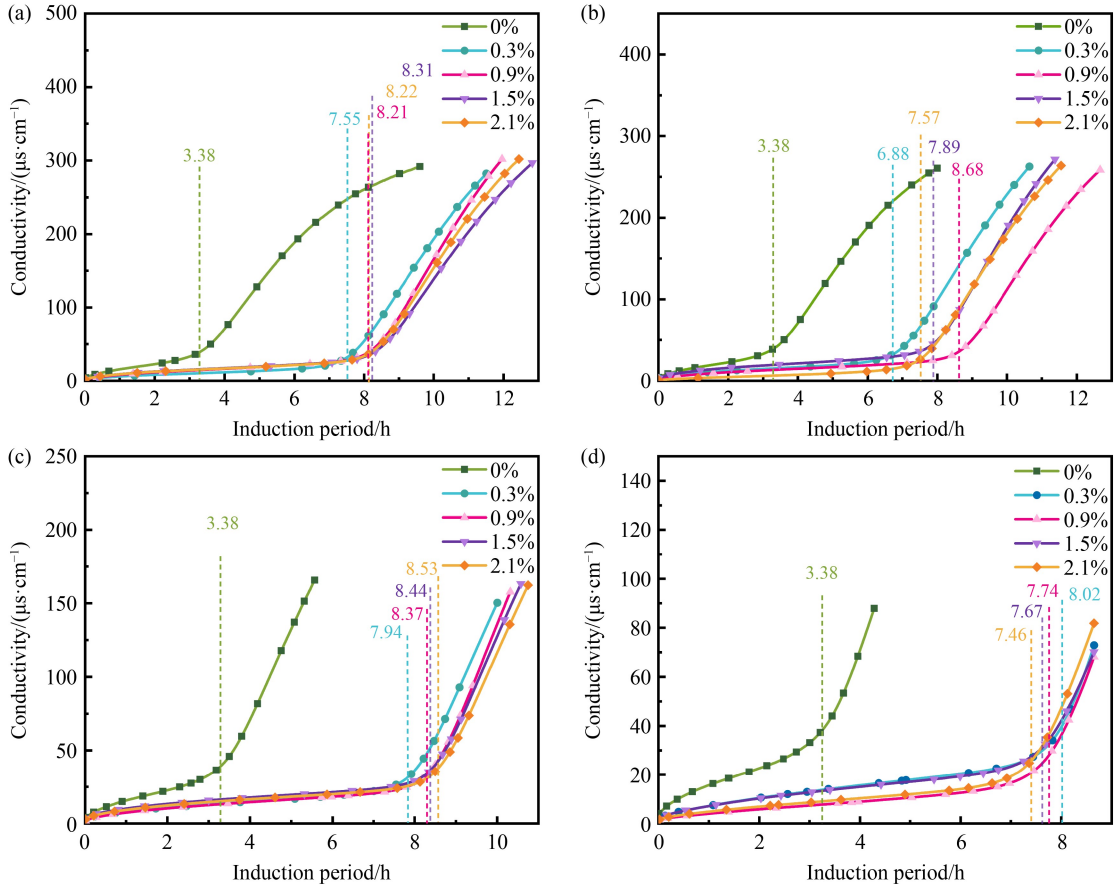

Fig. 8 Variation in the oxidation induction period of biodiesel. (a) EDTA; (b) HEDTA; (c) DTPA; (d) CDTA

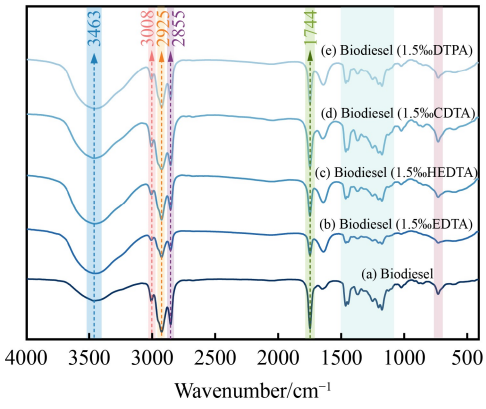

Fig. 9 Fourier spectrogram of biodiesel before and after treatment.

is attributed to the symmetric stretching of olefinic methylene groups and appears with relatively weak intensity. Peaks at 2855 and 2925 cm^{-1} represent the symmetric and asymmetric stretching of alkane methylene groups, respectively. A sharp and intense peak at 1744 cm^{-1} corresponds to the carbonyl group (C=O), indicating the presence of functional groups such as carboxylic acids, aldehydes, ketones, esters, anhydrides, and lactones. These results suggest that washing Jatropha biodiesel with chelating agents to remove alkaline earth metal ions does not alter its molecular structure.

3.5 Chelation mechanism

In addition to experimental investigations, theoretical quantum chemistry studies were conducted to explore the chelation mechanism of APCAs (HEDTA, EDTA, CDTA, DTPA) with alkaline earth metals. DFT calculations were performed to examine the complexation abilities, structural characteristics, and thermodynamic properties of metal-ligand complexes.

3.5.1 Electronic properties of APCAs

Molecular orbital calculations reveal distinct quantum chemical properties for the four APCAs. As shown in Fig. 10, the energy levels of the highest occupied molecular orbital (HOMO) follow the order of DTPA > CDTA > HEDTA > EDTA, while the lowest unoccupied molecular orbital (LUMO) energy levels follow the order of DTPA > HEDTA > EDTA > CDTA. The HOMO region is primarily localized around the nitrogen atom, while the LUMO region is distributed across the oxygen "arms." The non-uniform distribution of the LUMO is likely attributed to variations in the types and positions of oxygen atoms and the central nitrogen atom. The energy gap between the HOMO and LUMO reflects the chemical strength and reactivity of the molecule [50]. The energy gaps are ranked as EDTA > HEDTA > DTPA > CDTA. CDTA, exhibiting the smallest energy gap, is therefore more likely to participate in chelation reactions.

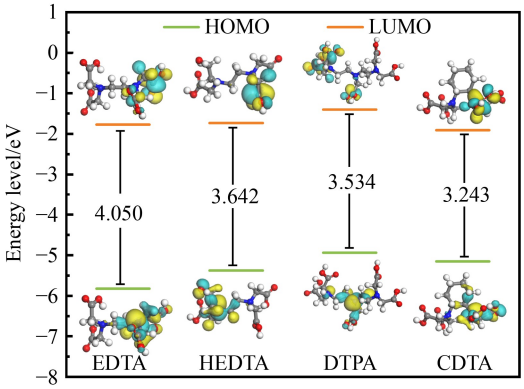

Fig. 10 HOMO-LUMO and energy gap values of chelating agents.

Other quantum chemical properties of APCA compounds are summarized in Table 5. The results indicate that Mg^{2+} has lower electronegativity than Ca^{2+}, making it more prone to accepting electrons donated by ligands. The electron affinity of the chelating agents follows the order of CDTA > EDTA > HEDTA > DTPA. All four compounds exhibit positive electron affinities, with CDTA demonstrating the greatest capacity to accept electrons. The global hardness values are ranked as EDTA > HEDTA > DTPA > CDTA, indicating that CDTA has the lowest hardness. This low hardness suggests that electrons in CDTA are more easily delocalized toward metal cations or surfaces, enhancing its chelation efficiency.

The optimized molecular structure and molecular

Table 5 Electron affinity, ionization energy, electronegativity, global hardness, and softness of chelating agents and metal ions (eV)

Chelating agent	Electron affinity EA	Ionization energy IP	Electronegativity χ	Global hardness η	Global softness σ
EDTA	1.773	5.823	3.798	2.025	0.494
HEDTA	1.734	5.376	3.555	1.821	0.549
DTPA	1.403	4.937	3.170	1.767	0.566
CDTA	1.910	5.153	3.532	1.621	0.617
Ca^{2+}	–11.441	–7.413	–9.427	2.0147	0.497
Mg^{2+}	–15.037	–9.102	–12.070	2.968	0.337

electrostatic potential (MEP) distributions of the four chelating agents are depicted in Fig. 11. The MEP analysis highlights the regions of notable chemical activity. Blue regions, indicating areas of negative electrostatic potential, are primarily concentrated around functional groups such as C=O, C–O, and $–NH_2$. These areas exhibit higher nucleophilicity and serve as potential electron donors. In contrast, red regions, indicating positive electrostatic potential, are located around carbon and hydrogen atoms, suggesting electrophilic behavior and electron-accepting capability.

Both carboxyl and amino groups coordinate with metal ions through their lone pairs of electrons, forming stable chelate ring structures. The carboxyl functional group, in particular, exhibit strong negative electrostatic potential, enabling them to form coordination bonds with positively charged metal ions (Ca^{2+}, Mg^{2+}) via electrostatic attraction. Oxygen atoms in the carboxyl groups possess high electron density and donate lone pairs of electrons to the empty orbitals of metal ions. Similarly, nitrogen atoms in the amino groups, residing in electron-rich regions, also carry lone pairs of electrons capable of directly coordinate with the empty orbitals of metal ions. This synergistic interaction between carboxyl and amino groups significantly enhances the stability of the resulting chelate structures formed with metal ions, thereby improving the effectiveness of the chelating agents in capturing and immobilizing metal ions.

3.5.2 Chelating agent complex analysis

During coordination, electron transfer occurs between the chelating agents and the metal ions, leading to a redistribution of electron density. The optimized structures and charge distributions of metal complexes formed with four chelating agents are shown in Fig. 12.

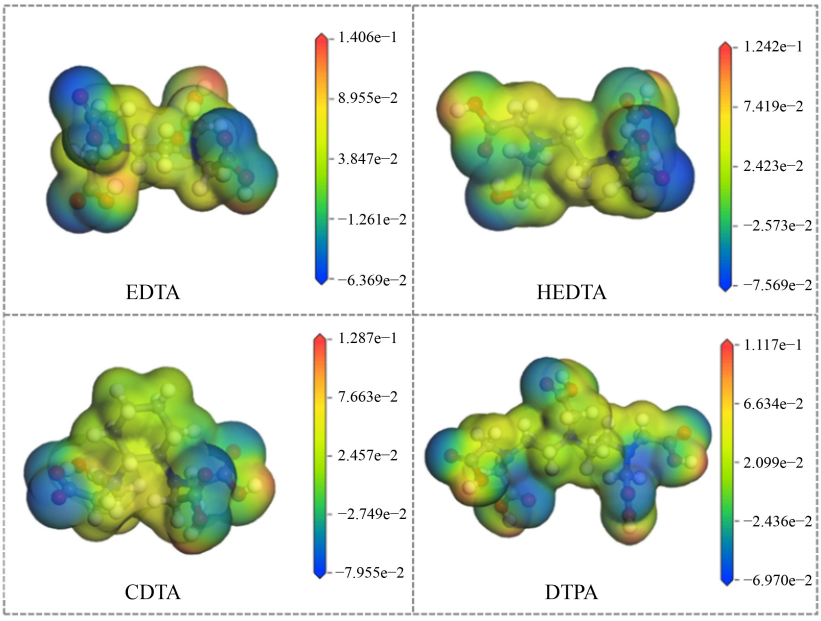

Fig. 11 Electrostatic potential of four APCAs.

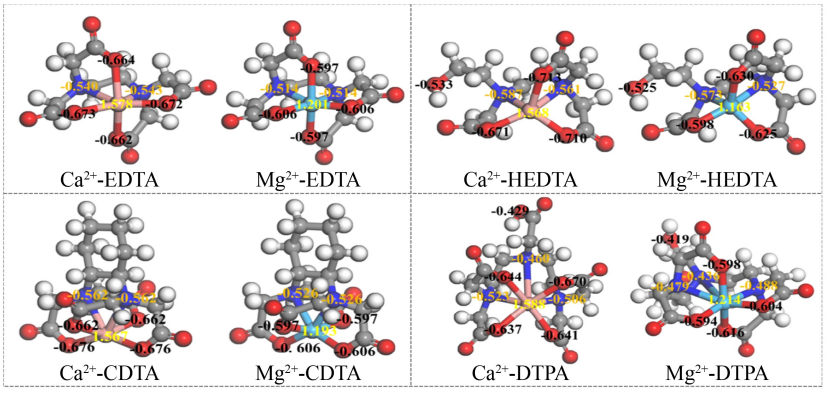

Fig. 12 Optimized structures and charge distributions of metal complexes with four chelating agents.

The Mulliken charges of the complexes show that the positive charge values of Ca^{2+} (1.578, 1.568, 1.588, and 1.193) are generally higher than those of Mg^{2+} (1.201, 1.631, 1.214, and 1.567) in the EDTA, HEDTA, DTPA, and CDTA complexes, respectively. Donor atoms (nitrogen and oxygen) coordinated to the central metal ions retain negative charges, with nitrogen atoms exhibiting less negative values compared to oxygen atoms.

For example, in the Ca^{2+}-EDTA complex, the Mulliken charges on nitrogen atoms are − 0.540 and − 0.543, while those on oxygen atoms are −0.664, −0.673, −0.662, and −0.672. Similarly, in the Mg^{2+}-EDTA complex, nitrogen atoms carry charge of −0.514, less negative than oxygen atoms (−0.597, −0.606, −0.597, and −0.606). This trend is consistent all examined complexes. These findings indicate that although both atom types contribute to coordination, charge transfer involving Ca^{2+} or Mg^{2+} is more favorable than with oxygen, suggesting that nitrogen atoms play a crucial role in stabilizing the metal-chelate complexes.

Figure 13 illustrates the HOMO/LUMO distributions and energy gap values (ΔE_{L-H}) of the metal complexes. ΔE_{L-H} values indicate that the Mg^{2+} complexes of EDTA, CDTA, and DTPA exhibit smaller ΔE_{L-H} values than their Ca^{2+} counterparts, suggesting greater stability. Among these, the Mg^{2+}-DTPA complex has the lowest ΔE_{L-H} value of 1.8655 eV. In contrast, for HEDTA, the Mg^{2+} complex displays a higher ΔE_{L-H} value than the Ca^{2+} complex, suggesting that while EDTA, CDTA, and DTPA form more stable complexes with Mg^{2+}, HEDTA favors the formation of a more stable complex with Ca^{2+}.

Figure 14 illustrates the electrostatic potential maps of complexes formed between the chelating agents and metal ions. Upon chelation, the electron density around the active sites (oxygen and nitrogen atoms) decreases, while the charge density around the metal ions increases, reflecting the redistribution of electrons during the chelation process. All eight complexes exhibit pronounced negative electrostatic potential regions, with the most intense negativity localized at the coordinating atoms. This distribution indicates a balanced electron transfer or sharing between the chelating agents and the metal ions. The negative potential regions highlight the specific atoms involved in electron donation, underscoring their role in forming stable coordination bonds with the metal ions.

3.5.3 Chelation process

In the deprotonated chelating agent molecules, multiple coordination atoms (N and O) simultaneously bind to a metal ion (M^{2+}), encapsulating it at the center, thereby forming a complex comprising multiple five-membered or six-membered rings. Figure 15 illustrates the proposed chelation process, as supported by quantum chemical calculations.

3.5.4 Interaction energy

The interaction energies of the four amino polycarboxylates with Ca^{2+} and Mg^{2+} were calculated to evaluate the binding strength the chelating agents and the metal ions. Figure 16 depicts the interaction energies, and Table 2 provides detailed numerical values. These calculations, performed in a vacuum and at the ground state, do not consider external factors such as kinetic energy, environmental conditions, concentration, pH, or solubility. Nonetheless, the results offer valuable insights

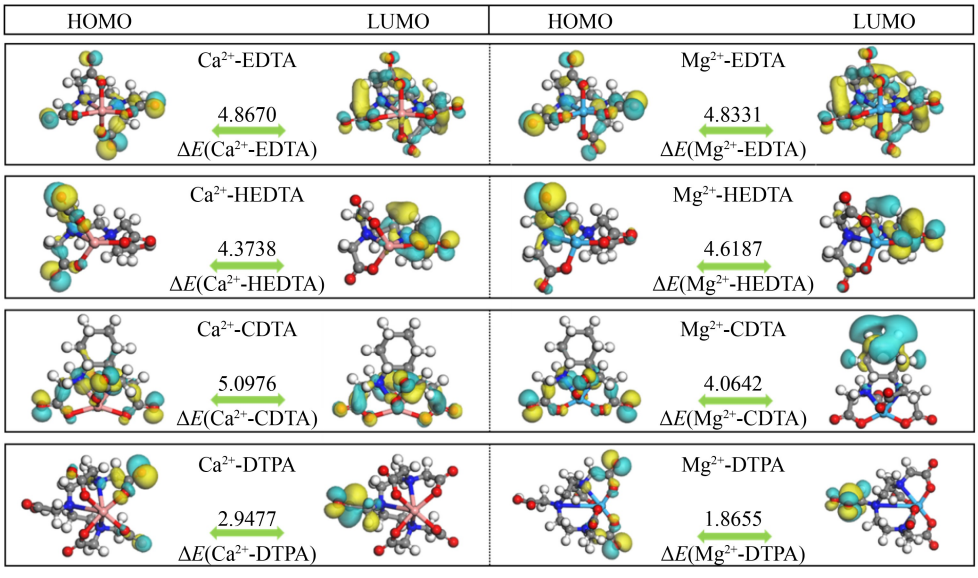

Fig. 13 HOMO-LUMO distributions and energy gap values of metal complexes.

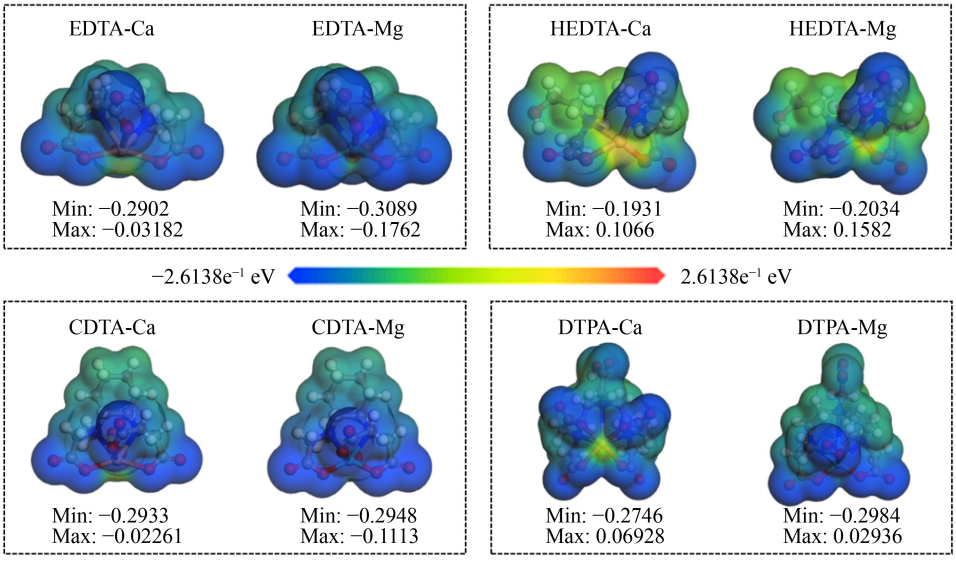

Fig. 14 Electrostatic potential maps of the complexes of four chelating agents with Ca^{2+} and Mg^{2+}.

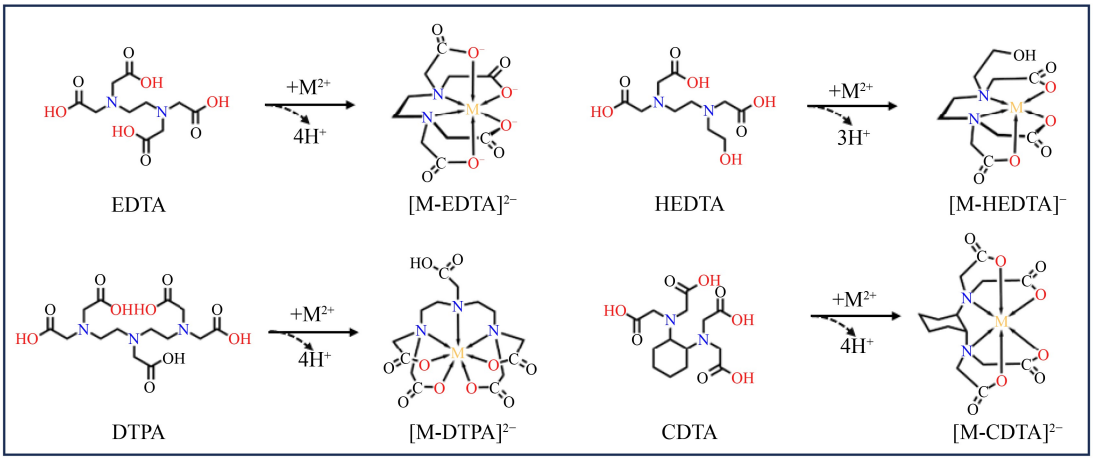

Fig. 15 Predicted chelation process.

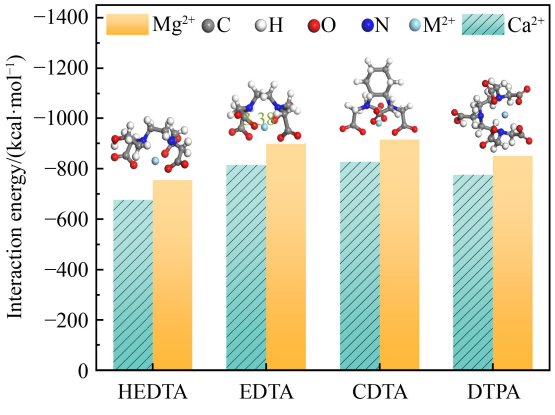

Fig. 16 Interaction energy and visualization of deprotonated APCAs with metal cations.

into the chelation mechanism and binding strength.

All interaction energies for all chelating agents with Ca^{2+} and Mg^{2+} are negative, indicating exothermic binding that promotes the formation of a more stable system. For Ca^{2+}, the interaction energy follows the order of HEDTA > DTPA > EDTA > CDTA. The same order is observed for Mg^{2+}. A more negative interaction energy signifies stronger chelation and the formation of a more stable complex. As the absolute value of the interaction energy (E_{int}) increases, the affinity between the chelating agent and the metal ion becomes stronger [51]. The results indicate that all four chelating agents exhibit stronger binding affinities for Mg^{2+} compared to Ca^{2+}. Furthermore, the absolute E_{int} values for CDTA and EDTA are higher than those for HEDTA and DTPA, demonstrating that EDTA and CDTA possess significantly greater affinities for both Ca^{2+} and Mg^{2+} relative to the other two chelating agents. These findings align closely with the experimental results.

These calculations provide deeper insights into the

mechanisms underlying chelating-agent-assisted metal extraction processes. Optimized molecular structures of the chelating agents and their corresponding chelation products were obtained. Frontier molecular orbitals (FMOs) of the chelating agents were analyzed to assess the relative reactivity. Molecular electrostatic potential (MEP) were used to visualize reactive sites, and interaction energies were calculated to quantify the strength of chelation.

4 Conclusions

This study demonstrated that APCAs can effectively extract alkaline earth metal ions (Ca^{2+} and Mg^{2+}) from biodiesel, substantially reducing the residual metal content. Among the four selected APCAs, CDTA exhibited the highest removal efficiency and selectivity for Ca^{2+} and Mg^{2+}, achieving rates of 98.6% and 94.3%, respectively, followed closely by EDTA, with removal efficiencies of 98.4% and 95.1% for Ca^{2+} and Mg^{2+}, respectively.

Moreover, the oxidation stability of Jatropha biodiesel treated with CDTA improved significantly, as the induction period increases from 3.38 to 8.68 h. After the chelating agents complexed the metal ions, the catalytic oxidation effect induced by metal ions on fatty acid methyl esters were significantly inhibited.

The molecular charge and electrostatic potential of the compounds were calculated using the DFT method in quantum chemistry, revealing that the main active sites of the four APCAs are the N atoms in amino groups and the O atoms in carboxyl groups. Based on frontier molecular orbital theory, CDTA has the smallest energy gaps and global hardness values, and the strongest interaction energies with Ca^{2+} and Mg^{2+}, reaching –826 and –915 kcal/mol, respectively.

These findings confirm that APCAs are effective in reducing alkaline earth metal content in biodiesel while preserving its essential functional properties.

Acknowledgements This work was financially supported by Yunnan Fundamental Research Projects, China (Grant No.202201AS070036), the National Natural Science Foundation of China (Grant No. 52166013), Major Science and Technology Project of Yunnan Province, China (Grant Nos. 202302AF080005, 202302AG050011, 202302AQ370003), Technology Talent and Platform Plan of Yunnan Province, China (Grant No. 202305AS350016).

Competing Interests The authors declare that they have no competing interests.

References

1. Khalaf M, Qenawy M, Xuan T. Experimental investigation on the performance and emissions of extracted biodiesels from mixed Jatropha-Castor seeds: Comprehensive assessment. Applied Energy, 2024, 374: 124022
2. Han D, Zhai J, Duan Y, et al. Macroscopic and microscopic spray characteristics of fatty acid esters on a common rail injection system. Fuel, 2017, 203: 370–379
3. Andrade M C, Gorgulho Silva C O, de Souza Moreira L R, et al. Crop residues: Applications of lignocellulosic biomass in the context of a biorefinery. Frontiers in Energy, 2022, 16(2): 224–245
4. Wang C, Li T, Xu W, et al. Recent advances in co-processing biomass feedstock with petroleum feedstock: A review. Frontiers in Energy, 2024, 18(6): 735–759
5. Ai W, Cho H M, Mahmud M I. The impact of various factors on long-term storage of biodiesel and its prevention: A review. Energies, 2024, 17(14): 3449
6. Khan I U. Biodiesel production and selected fuel qualities from prospective non-edible oils: Hevea brasiliensis, Madhuca longifolia, Azadirachta indica, and Gossypium hirsutum. International Journal of Green Energy, 2024, 21(13): 3054–3071
7. Knothe G, Steidley K R. Lubricity of components of biodiesel and petrodiesel. The origin of biodiesel lubricity. Energy & Fuels, 2005, 19(3): 1192–1200
8. Morajkar P P, Abdrabou M K, Raj A, et al. Transmission of trace metals from fuels to soot particles: An ICP-MS and soot nanostructural disorder study using diesel and diesel/Karanja biodiesel blend. Fuel, 2020, 280: 118631
9. Han D, Wang C, Duan Y, et al. An experimental study of injection and spray characteristics of diesel and gasoline blends on a common rail injection system. Energy, 2014, 75: 513–519
10. Duan Y, Liu W, Huang Z, et al. An experimental study on spray auto-ignition of RP-3 jet fuel and its surrogates. Frontiers in Energy, 2021, 15(2): 396–404
11. Wang L, Wang H, Fan J, et al. Synthesis, catalysts and enhancement technologies of biodiesel from oil feedstock—A review. Science of the Total Environment, 2023, 904: 166982
12. Matsuoka K, Hasegawa S, Yuma T, et al. Application of foam separation method for removal of alkaline earth metal ions from solution. Journal of Molecular Liquids, 2019, 294: 111663
13. Yu C, Thy P, Wang L, et al. Influence of leaching pretreatment on fuel properties of biomass. Fuel Processing Technology, 2014, 128: 43–53
14. Cui H, Turn S Q, Tran T, et al. Mechanical dewatering and water leaching pretreatment of fresh banagrass, guinea grass, energy cane, and sugar cane: Characterization of fuel properties and byproduct streams. Fuel Processing Technology, 2015, 139: 159–172
15. Gao X, Hu Y, Guo T, et al. Comparative study of the competitive adsorption of Mg, Ca and Sr ions onto resins. Adsorption Science and Technology, 2013, 31(1): 45–58
16. Luo L, Li F, Zhang H. Efficient removal of alkali and alkaline earth metals from biodiesel using ion-exchange resin: Performance and mechanism. Separation and Purification Technology, 2023, 323: 124485
17. Wang L, Lin S. Mechanism of selective ion removal in membrane capacitive deionization for water softening. Environmental Science & Technology, 2019, 53(10): 5797–5804
18. Morgan G T, Drew H D K. Researches on residual affinity and

co-ordination. Part II. Acetylacetones of selenium and tellurium. Journal of the Chemical Society Transactions, 1920, 117(0): 1456–1465

19. Arun Y, Daifa M, Domb A J. Polyhydroxamic acid as an efficient metal chelator and flocculant for wastewater treatment. Polymers for Advanced Technologies, 2021, 32(2): 842–852
20. Zulkernain N H, Uvarajan T, Ng C C. Roles and significance of chelating agents for potentially toxic elements (PTEs) phytoremediation in soil: A review. Journal of Environmental Management, 2023, 341: 117926
21. Kim J J, Kim Y S, Kumar V. Heavy metal toxicity: An update of chelating therapeutic strategies. Journal of Trace Elements in Medicine and Biology, 2019, 54: 226–231
22. Hassan A, Mahmoud M, Bageri B S, et al. Applications of chelating agents in the upstream oil and gas industry: A review. Energy & Fuels, 2020, 34(12): 15593–15613
23. Kamal M S, Hussein I, Mahmoud M, et al. Oilfield scale formation and chemical removal: A review. Journal of Petroleum Science Engineering, 2018, 171: 127–139
24. Wang K S, Resch R, Dunn K, et al. Dissolution of the barite (001) surface by the chelating agent DTPA as studied with non-contact atomic force microscopy. Colloids and Surfaces. A, Physicochemical and Engineering Aspects, 1999, 160(3): 217–227
25. Li N, He D, Zhao L, et al. An alkaline barium- and strontium-sulfate scale dissolver. Chemistry and Technology of Fuels and Oils, 2016, 52(2): 141–148
26. Edmunds C W, Hamilton C, Kim K, et al. Using a chelating agent to generate low ash bioenergy feedstock. Biomass and Bioenergy, 2017, 96: 12–18
27. Sorour M H, Hani H A, Shaalan H F, et al. Experimental screening of some chelating agents for calcium and magnesium removal from saline solutions. Desalination and Water Treatment, 2016, 57(48-49): 22799–22808
28. Abu-El-Halawa R, Zabin S A. Removal efficiency of Pb, Cd, Cu and Zn from polluted water using dithiocarbamate ligands. Journal of Taibah University for Science: JTUSCI, 2017, 11(1): 57–65
29. Sebastian A, Prasad M N V. Vertisol prevent cadmium accumulation in rice: Analysis by ecophysiological toxicity markers. Chemosphere, 2014, 108: 85–92
30. Pinto I S S, Neto I F F, Soares H M V M. Biodegradable chelating agents for industrial, domestic, and agricultural applications—A review. Environmental Science and Pollution Research International, 2014, 21(20): 11893–11906
31. Zhou L, Li F, Wang W. Determination of total phosphorus in biodiesel by ion chromatography. Microchemical Journal, 2021, 162: 105875
32. Sendzikiene E, Makareviciene V, Janulis P. Oxidation stability of biodiesel fuel produced from fatty wastes. Polish Journal of Environmental Studies, 2005, 14: 335–339
33. Zheng Y, Li F, Zhang H, et al. Fishhook characteristics of biodiesel lubricity during autoxidation. Fuel, 2023, 331: 125897
34. Ridzwan M H, Yaakob M K, Zabidi Z M, et al. Computational insight into the quantum chemistry, interaction and adsorption energy of aminopolycarboxylic acid chelating agents towards metal cations. Computational & Theoretical Chemistry, 2022, 1208: 113579
35. Mahmoud M, Attia M, Al-Hashim H. EDTA chelating agent/seawater solution as enhanced oil recovery fluid for sandstone reservoirs. Journal of Petroleum Science Engineering, 2017, 152: 275–283
36. Martell A E, Calvin M. Chemistry of the metal chelate compounds. Soil Science, 1952, 74(5): 403
37. Smith R, Martell A, Motekaitis R, et al. NIST critically selected stability constants of metal complexes. NIST Standard Reference Database 46, version 8.0. U.S. Department of Commerce: Washington, DC, 2004
38. Yoe J H. Chemistry of the metal chelate compounds. Journal of Chemical Education, 1953, 30(4): 215
39. Onawole A T, Hussein I A, Nimir H I, et al. Molecular design of novel chemicals for iron sulfide scale removal. Journal of Chemistry, 2021:7698762
40. Onawole A T, Hussein I A, Sultan A, et al. Molecular and electronic structure elucidation of Fe^{2+}/Fe^{3+} complexed chelators used in iron sulphide scale removal in oil and gas wells. Canadian Journal of Chemical Engineering, 2019, 97(7): 2021–2027
41. Azzam E M S, Gad E A M, Al-Fahemi J H. Experimental and theoretical study on triazole derivatives as chelating agents to remove Fe^{++} ions from wastewater in oil field. Journal of Heterocyclic Chemistry, 2020, 57(6): 2586–2596
42. Delley B. An all-electron numerical method for solving the local density functional for polyatomic molecules. Journal of Chemical Physics, 1990, 92(1): 508–517
43. Delley B. From molecules to solids with the $DMol_3$ approach. Journal of Chemical Physics, 2000, 113(18): 7756–7764
44. Becke A D. A multicenter numerical integration scheme for polyatomic molecules. Journal of Chemical Physics, 1988, 88(4): 2547–2553
45. Lee Y, Yang W, Parr R G. Development of the Colle-Salvetti correlation-energy formula into a functional of the electron density. Physical Review B: Condensed Matter, 1988, 37(2): 785–789
46. Fredd C N, Fogler H S. The influence of chelating agents on the kinetics of calcite dissolution. Journal of Colloid and Interface Science, 1998, 204(1): 187–197
47. Du J, Su L, Zhang D, et al. Experimental investigation into the pore structure and oxidation activity of biodiesel soot. Fuel, 2022, 310: 122316
48. Sui M, Chen Y, Li F, et al. Study on transition metal ion Fe^{3+} catalyzed biodiesel oxidation and inhibition mechanism. Fuel, 2021, 303: 121288
49. Amran N A, Bello U, Hazwan Ruslan M S. The role of antioxidants in improving biodiesel's oxidative stability, poor cold flow properties, and the effects of the duo on engine performance: A review. Heliyon, 2022, 8(7): e09846
50. Kerru N, Gummidi L, Bhaskaruni S V H S, et al. A comparison between observed and DFT calculations on structure of 5-(4-chlorophenyl)-2-amino-1,3,4-thiadiazole. Scientific Reports, 2019, 9(1): 19280
51. Nowack B. Environmental chemistry of aminopolycarboxylate chelating agents. Environmental Science & Technology, 2002, 36(19): 4009–4016